

Divide and Conquer Partition for Fourier Reconstruction Sparse Inversion with its Applications

Zhaolin ZHU, Haoran REN*, Liurong TAO, Jinsheng JIANG, Tong WANG, Mingxin CHENG, Shuaimin DING, Rui DU

Abstract: A partition method, with an efficient divide and conquer partition strategy, for the non-uniform sampling signal reconstruction based on Fourier reconstruction sparse inversion (FRSI) is developed. The novel partition FRSI(P-FRSI) is motivated by the observation that the partition processing of multi-dimensional signals can reduce the reconstruction difficulty and save the reconstruction time. Moreover, it is helpful to choose suitable reconstruction parameters. The P-FRSI employs divide and conquer strategy, and the signal is firstly partitioned into some blocks. Following that, traditional FRSI is applied to reconstruct signals in each block. We adopt linear or nonlinear superposition to determine the weight coefficients during integrating these blocks. Finally, P-FRSI is applied to two-dimensional seismic signal reconstruction. The superiority of the new method over conventional FRSI is demonstrated by numerical reconstruction experiments.

Keywords: Divide and conquer partition; Fourier reconstruction sparse inversion; Non-uniform sampling; Signal reconstruction

1 INTRODUCTION

In many applications, the signal inherently might be generated by non-uniform sampling [1]. For instance in seismic signal acquisition, the non-uniform sampling usually occurs on the offshore survey geometry for feather floating, cost control, and dead traces [2]. The seismic data reconstruction is essential for seismic data processing workflow. However, most of the traditional reconstruction algorithms cannot effectively and exactly deal with non-uniform sampling signals [3]. To solve this problem, numerous non-uniformly reconstruction algorithms have been raised. These algorithms can be classified into three categories: operators-based [4], prediction error filter (PEF)-based [5], transformation-based [6-8], and machine learning-based [9-11] reconstruction.

Operators-based reconstruction offers a theoretically attractive framework because noises from non-uniform sampling can be suppressed by weighted summation or adopting an inversion approach [12]. This kind of algorithm typically is computationally expensive. PEF-based reconstruction interpolates by filtering with a minimum error filter in the spatial domain [13]. Domain-transformed reconstruction needs to request the coefficients of one transform such as Fourier, Tau-p, seislet, wavelet that generate the signal on the non-uniform grid [14-16]. Most of them are efficient enough for reconstruction if the transformation is fast [17]. Besides the above three categories of traditional algorithms, some new reconstruction algorithms are proposed. For example, in terms of spectral efficiency and energy consumption, Font-Segura and Vázquez solved the problem of non-uniformly sampling's spectral analysis and spectrum sensing by taking advantage of Bernoulli sampling [18]. Feizi and Angelopoulos investigated the power efficiency aspects of non-uniform sampling [19].

Among transformation-based reconstruction algorithms, extensive attention is paid to Fourier reconstruction due to its computation efficiency [20]. The underlying basis of these algorithms is by posing the reconstruction as an inverse problem where, from a non-uniform sampling signal, one tries a way to recover the Fourier transform coefficients of the reconstructed signal

[21]. Different criteria to solve such an inversion problem are discussed by several researchers. For example, Liu introduced a minimum weighted norm interpolation criterion to solve the inverse problem [22]. Sacchi and Ulrych derived a Cauchy criterion to build high-resolution coefficients of the reconstructed signal in the discrete Fourier domain [23]. Wang solved the inverse problem with a particular constraint criterion, referred to as sparseness constrained least squares [24]. In addition, Duijndam and Schonewille et al. presented a Fourier reconstruction minimum norm (FRMN) criteria [15, 25].

Considering that FRMN yet has some limitations, Fourier reconstruction sparse inversion (FRSI), an improved algorithm of FRMN is proposed [26, 27]. By introducing sparse constraint and non-quadratic weight function, FRSI can obtain better performance than FRMN. Notwithstanding FRSI is very useful for reconstruction, but there are also some drawbacks in practical application as follows: (a) it is inconvenient to choose optimal parameters for large-size signal reconstruction; (b) curved lines are prone to errors; (c) it is not a time-saving method.

To overcome the above limitations of FRSI, a novel partition FRSI(P-FRSI) is proposed. This method employs a "divide and conquer" strategy, and reconstructs every sub-block after dividing the given signal into many sub-blocks. Finally, the reconstruction results of every sub-block are spliced. The subsequent tests validated the advantages of P-FRSI.

The rest of this paper is organized as follows. Section 2 outlines the traditional FRSI. Then we illustrate our motivation to improve the algorithm in Section 3. And the implementation of the partition method for FRSI is introduced in Section 4. Section 5 shows the experimental results, and gives the conclusions and some discussions in Section 6.

2 OVERVIEW ON FOURIER RECONSTRUCTION SPARSE INVERSION

2.1 Non-Uniform Discrete Fourier Transform

The discrete Fourier transform (DFT) [28] differs from the continuous Fourier transform and it transforms a finite digital signal to the counterpart in the wave number domain.

Given the discrete signal at uniform grids $[0, \Delta x, 2\Delta x, \dots, (N-1)\Delta x]$, its DFT is:

$$\tilde{p}_{DFT}[k] = \sum_{n=0}^{N-1} p[n] e^{\frac{j\pi}{N} n k} \quad (1)$$

where, m is the index of wave number. If the sampling interval in the wave number domain is set to $\Delta\gamma$, uniform wave number values are listed as $[0, \Delta\gamma, 2\Delta\gamma, \dots, (N-1)\Delta\gamma]$ and N is equal to $2\pi/\Delta\gamma\Delta x$.

Δx must meet the Nyquist sampling theorem [29] to suppress signal aliasing of DFT.

When the sampled locations are replaced by actual sample locations (non-uniformly sampled) $[x_0, x_1, x_2, \dots, x_{N-1}]$, the non-uniform DFT (NDFT) should be instead applied to get the Fourier coefficients. The NDFT is expressed as the following formula:

$$\tilde{p}_{NDFT}[k\Delta\gamma] = \sum_{n=0}^{N-1} p[x_n] e^{jm\Delta\gamma x_n} \Delta x_n \quad (2)$$

with $\Delta x_n = (x_{n+1} - x_{n-1})/2$.

The wavenumber in the Fourier domain is limited to the spatial bandwidth $[-M\Delta\gamma, M\Delta\gamma]$ with $\Delta\gamma = 2\pi/(x_{N-1} - x_0)$. The inverse transform which is obtained from DFT coefficients \tilde{p}_{DFT} :

$$p[x_n] = \frac{\Delta\gamma}{2\pi} \sum_{m=-M}^M \tilde{p}_{DFT}[m\Delta\gamma] e^{-jm\Delta\gamma x_n} \quad (3)$$

Duijndam and Schonewille proposed a new approach to compute the NDFT coefficients [30]. They found that the NDFT coefficients were exactly equal to the DFT coefficients and the NDFT sampling weight (sampling interval):

$$\begin{aligned} \tilde{p}_{NDFT}[m\Delta\gamma] &= \\ &= \frac{\Delta\gamma}{2\pi} \sum_n \sum_q \tilde{p}_{DFT}[q\Delta\gamma] e^{-jq\Delta\gamma x_n} e^{jm\Delta\gamma x_n} \Delta x_n = \\ &= \frac{\Delta\gamma}{2\pi} \sum_n \sum_q \Delta x_n e^{j(m-q)\Delta\gamma x_n} \tilde{p}_{DFT}[q\Delta\gamma] = \\ &= \{PSF \cdot \tilde{p}_{DFT}\}[m\Delta\gamma] \end{aligned} \quad (4)$$

PSF represents the "point spread function" [31] and here is set as the spatial weights of NDFT. The PSF is defined as the following formula:

$$PSF[m\Delta\gamma] = \frac{\Delta\gamma}{2\pi} \sum_{n=0}^{N-1} \Delta x_n e^{jm\Delta\gamma x_n} \quad (5)$$

2.2 Fourier Reconstruction Sparse Inversion (FRSI)

The distortion size in NDFT depends on the PSF. Feichtinger [32] and Duijndam [15] found that in the

reconstruction step, a logical method for deconvolution calculation of PSF was included. They devised a strategy for solving the problem, which is to minimize the loss function [27]:

$$E = \frac{1}{\sigma_n^2} \|W^{1/2}(p - L\tilde{p})\|_2^2 + \mu(\tilde{p}) \quad (6)$$

On the right-hand side of Eq. (6), the first part is the fitting observed data and calculated data, and the second part is the model constraint term, where:

$$p_n = p[x_n] \quad (7)$$

$$\tilde{p}_m = \tilde{p}_{DFT}[m\Delta\gamma] \quad (8)$$

$$L_{nm} = \frac{\Delta\gamma}{2\pi} e^{-jm\Delta\gamma x_n} \quad (9)$$

$$W_{nn} = \Delta x_n \quad (10)$$

$$\mu(\tilde{p}_m) = \frac{1}{2(1-\alpha)} (\tilde{p}_m^2 + 1)^{1-\alpha} \quad (11)$$

The minimum of the loss function in Eq. (6) is written as:

$$\hat{\tilde{p}} = (L^H WL + \sigma_n^2 C_{\tilde{p}})^{-1} L^H Wp \quad (12)$$

with:

$$[C_{\tilde{p}}]_{mm} = (\sigma_p^2 + \tilde{p}_m^* \tilde{p}_m)^\alpha \quad (13)$$

The loss function Eq. (6) which includes the non-quadratic model constraint term, yields an estimator of sparse inversion. Any non-quadratic penalty function which has been already utilized in robust regression can be applied for the constraint term. As we all know, no penalty function is best for all experiments. We must choose different penalty functions in different conditions.

Since choosing a different model of penalty function has ambiguity, we set a new function for weighting value, and describe it in the above Eq. (8), to adjust the sparsity by using the scale α (distribution of the model parameter). For $\alpha = 1/2, 1, 2$, the weight functions are I_{1-2} [33], Cauchy and Geman-McClure types respectively. The scalars σ_n^2 and σ_p^2 denote the noise variances and the signal variances.

In a real application, the variances are applied simply as inversion tuning weights. We can substitute a damping parameter $\lambda I = \sigma_n^2 / \sigma_p^2 I$ for the term $\sigma_n^2 C_{\tilde{p}}$ among all cases of minimum-norm optimization problems [15]. The stabilization factor $\lambda = \sigma_n^2 / \sigma_p^2$ which can be demonstrated by Parseval's relation (15 appendix), can be approximated by:

$$\lambda = \sigma_n^2 / \sigma_p^2 = F \frac{\Delta\gamma}{2\pi} \frac{M_p}{N} \quad (14)$$

with $M_p = 2M + 1$ is the total number of DFT coefficients in the positive and negative directions, and F stands for the excepted ratio between signal to noise. The tuning parameter σ_p^2 can tune the sparsity. A good experience is to make σ_p^2 percentages of the maximal value in all the squared coefficients of NDFT:

$$\sigma_p^2 = Q\% \times \left\| \max \left\{ \sum_{n=0}^{N-1} p[x_n] e^{jm\Delta\gamma x_n} \Delta x_n \right\} \right\|_2^2 \quad (15)$$

and $\sigma_n^2 = \lambda \times \sigma_p^2$, therefore, we can optimize the reconstruction result through tuning the parameter $Q\%$.

The above inversion can be implemented by using the conjugate gradient method which utilizes the Toeplitz matrix in the normal equation. The linear system is brought and thus, is solved by a preconditioned conjugate gradient method with $C_{\tilde{p}}$ which is regarded as a precondition factor. Preconditioning can accelerate the inversion by reducing the iteration number for convergence. Zwartjes represents the loss function of Eq. (6) as a likelihood estimation form [27] and then through a standard Z transformation it becomes:

$$J = \frac{1}{\sigma_n^2} \|W^{1/2}(p - L'z)\|_2^2 + \|z\|_2^2 \quad (17)$$

with $z = C_{\tilde{p}}^{-1/2}\tilde{p}$ and $L' = LC_{\tilde{p}}^{1/2}$. The estimated results are attained by solving the optimization problem of Eq. (17). The results are:

$$\tilde{z} = (L^H WL' + \sigma_n^2 I)^{-1} L^H W p \quad (18)$$

The solutions are given in Eq. (19):

$$\begin{aligned} \hat{p}_{FRSI} &= C_{\tilde{p}}^{1/2} \left(C_{\tilde{p}}^{1/2} L^H WL C_{\tilde{p}}^{1/2} + \sigma_n^2 I \right)^{-1} \\ &\quad C_{\tilde{p}}^{1/2} L^H W y \end{aligned} \quad (19)$$

and now we can solve Eq. (19) via iteratively reweighted least squares (IRLS), which need repeatedly utilizing the conjugate gradient for normal equations (CGNE) method to the linearized equations, followed by updating results of the nonlinear system. See Zwartjes and Sacchi for a detailed description of IRLS with preconditioned CGNE [26]. We found the system tends to be stable after four iterations approximately.

We have got the results through Eq. (18) in the wavenumber domain, and the constructed signal in the spatial domain p_r is easily written as:

$$p_r = L_r \times \hat{p}_{FRSI} \quad (20)$$

with the coefficient matrix L_r which is similar to the definition in Eq. (9).

3 MOTIVATION FOR DIVIDE AND CONQUER PARTITION METHOD

3.1 Reduce the Reconstruction Difficulty by Linearizing Curved Events

FRSI performs better than handling curved lines when dealing with straight lines. Most reconstructive errors occur during curved line reconstruction. Hence, the performance of FRSI will be improved if the signal is linearized.

Usually, there are a lot of curved lines in multidimensional seismic signals which cannot be reconstructed well. Fig. 1 shows that one curved seismic trace is divided into some parts. The blue dotted line is the original signal and the red solid line is composed of the segmented line segments. For getting a better view, the whole red straight-line segments have shifted down 0.2 units. The whole signal is curved and instead seems to be straight in each part. If this curved line was partitioned into more separate segments, each segment could be approximated as a straight line. Therefore, linearization can be done by partitioning the line.

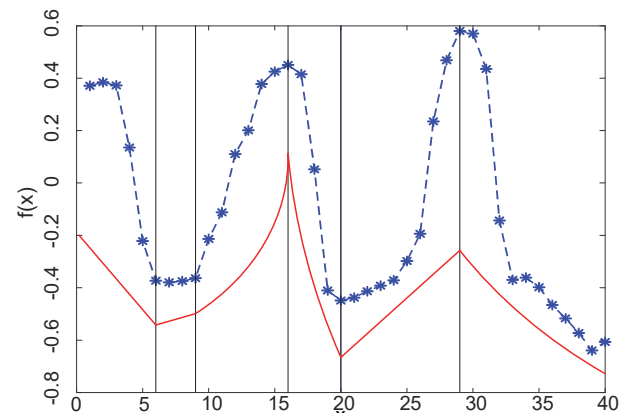


Figure 1 Converting a curved trace to straight-line segments

3.2 Saving Reconstruction Time

Usually, one 2-D seismic planar signal has $N_t \times N_x$ sampling points. When calculating the spectrum of the signal by Eq. (19), it requires numerous computations on a matrix such as multiplication and inverse. The time assuming is unaffordable when the size of the matrix becomes large. In addition, FRSI reconstructs the 2-D signals of each trace respectively and then puts them together to get the whole reconstructive result. Thus, the computational cost of reformulated FRMN is too high to burden.

An experiment is designed. We generate 4 groups of 10 stochastic matrixes in a MATLAB environment. The size of the matrix is set to 1000×1000 , 500×500 , 250×250 , and 125×125 in 4 groups. Take Group two and three, for example, the whole data in Group two is 4 times larger than the data in Group three. It consumed 2.16 seconds to calculate these matrix inversions in Group two. However, it only consumed 0.39 seconds in Group

three. As a consequence, it only spent about one-sixth of the time handling one-fourth of the matrix inversion calculation. Therefore, partition methods can help us to save the runtime of the algorithm.

4 PROPOSED PARTITION METHOD FOR FRSI

4.1 Partition Multi-Dimensional Signal Into Sub-Blocks

The schematic diagram of partition methods that are used in planar seismic data is shown in Fig. 2. The size of the 2-D signal is $N_t \times N_x$, where N_t and N_x are sampling points on the time and spatial direction respectively. The seismic signals have a distinguishing characteristic that they are mainly transverse, so we can divide more sub-blocks in the spatial direction for the sake of getting the linearized result.

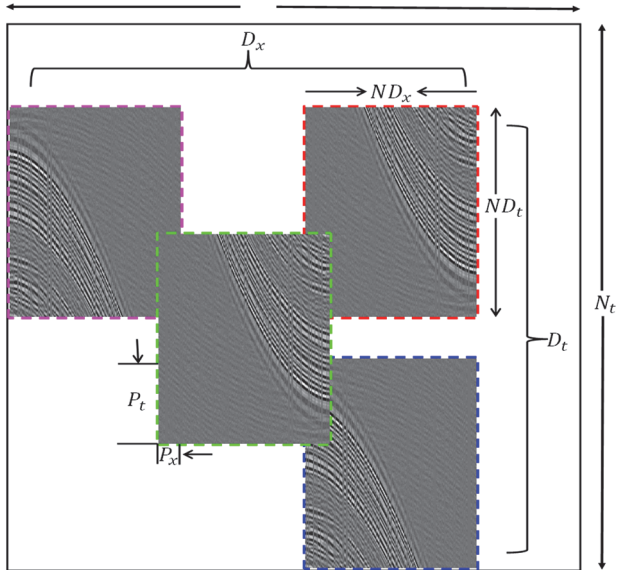


Figure 2 Partition methods for FRSI in 2-D signal

As seen in Fig. 2, in the spatial direction the data were divided into D_x sub-blocks, each sub-block has ND_x sampling points. There are P_x overlapped lengths that can be used for avoiding aliasing and edge-effect between each sub-block. If there was no P_x length between each sub-block, likely, these "sub-blocks" can still be seen clearly when observing the reconstruction results obtained by the

P-FRSI algorithm. For calculating ND_x conveniently, Eq. (21) can be adapted into Eq. (22).

$$N_x + P_x \times (D_x - 1) = ND_x \times D_x \quad (21)$$

$$ND_x = \frac{N_x + P_x \times (D_x - 1)}{D_x} \quad (22)$$

Similarly, on the time direction the signals were divided into D_t sub-blocks, each sub-block has ND_t sampling points. So the size of each sub-block is:

$$ND_t \times ND_x$$

$$N_t + P_t \times (D_t - 1) = ND_t \times D_t \quad (23)$$

$$ND_t = \frac{N_t + P_t \times (D_t - 1)}{D_t} \quad (24)$$

Now FRSI can reconstruct the seismic signal in each sub-block, but they were not the final result.

4.2 Determining the Weight Coefficients Between Blocks

The final reconstruction result needs to be formed by stitching the reconstruction results of each sub-block. Due to reserving of P_x overlapped lengths, the linear or nonlinear superposition method can be used to solve the aliasing problems during stitching them together. The schematic diagram is shown in Fig. 3.

Taking linear superposition using pink block (B1 + B2) and yellow block (B2 + B3 + B4) as an example, a regularly weighted calculation was required to be done on each block firstly: the P_x overlapped lengths must multiply linear weighted coefficients. Secondly, blocks with multiplying weighted coefficients (as shown in the weighted superposition formula given in Fig. 3) were added together to get the final result gray block (B6).

The linear superposition was usually used to determine the weighted coefficients. Of course, if the block on the left (e.g. yellow block) has an exactly higher level of performance than the block on the right (e.g. green block (B4 + B5)), nonlinear superposition should be used.

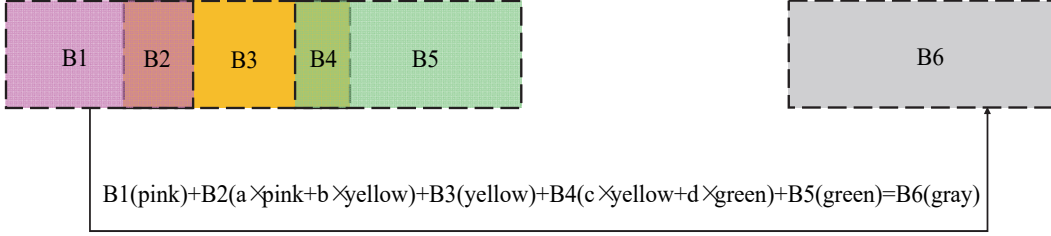


Figure 3 Linear or nonlinear superposition to determine the weight coefficients between blocks

5 EXPERIMENTS

The following are two illustrative examples of FRSI and P-FRSI that are applied in 2-D seismic signal reconstruction.

5.1 Linear Planar Seismic Signal Reconstruction

For convenience, the first example is started with a simple 2-D linear planar signal. Fig. 4a shows this synthetic linear event. The window's size of it is 2000 ms and 1600 traces in the spatial dimension. In this example,

the time interval is 4ms and the trace spacing is 10m, so this composite signal contains 500×160 points. After the manual setting, the data of the 50 traces in the original 160 traces are deleted randomly. Fig. 4c shows the FRSI reconstruction results, which σ_p^2 was set as the 50th percentile of the squared NDFT coefficients and 5 IRLS iterations, and other values $a = 1$, $Mkx = 11$ (frequency

bandwidth) were used which were hand-picked to get the best result.

It can be seen from Fig. 4c that the reconstruction quality of FRSI in the middle part is better than that in the left and right boundary part. Now, to improve the performance of FRSI, the linear events are reconstructed again with partition methods.

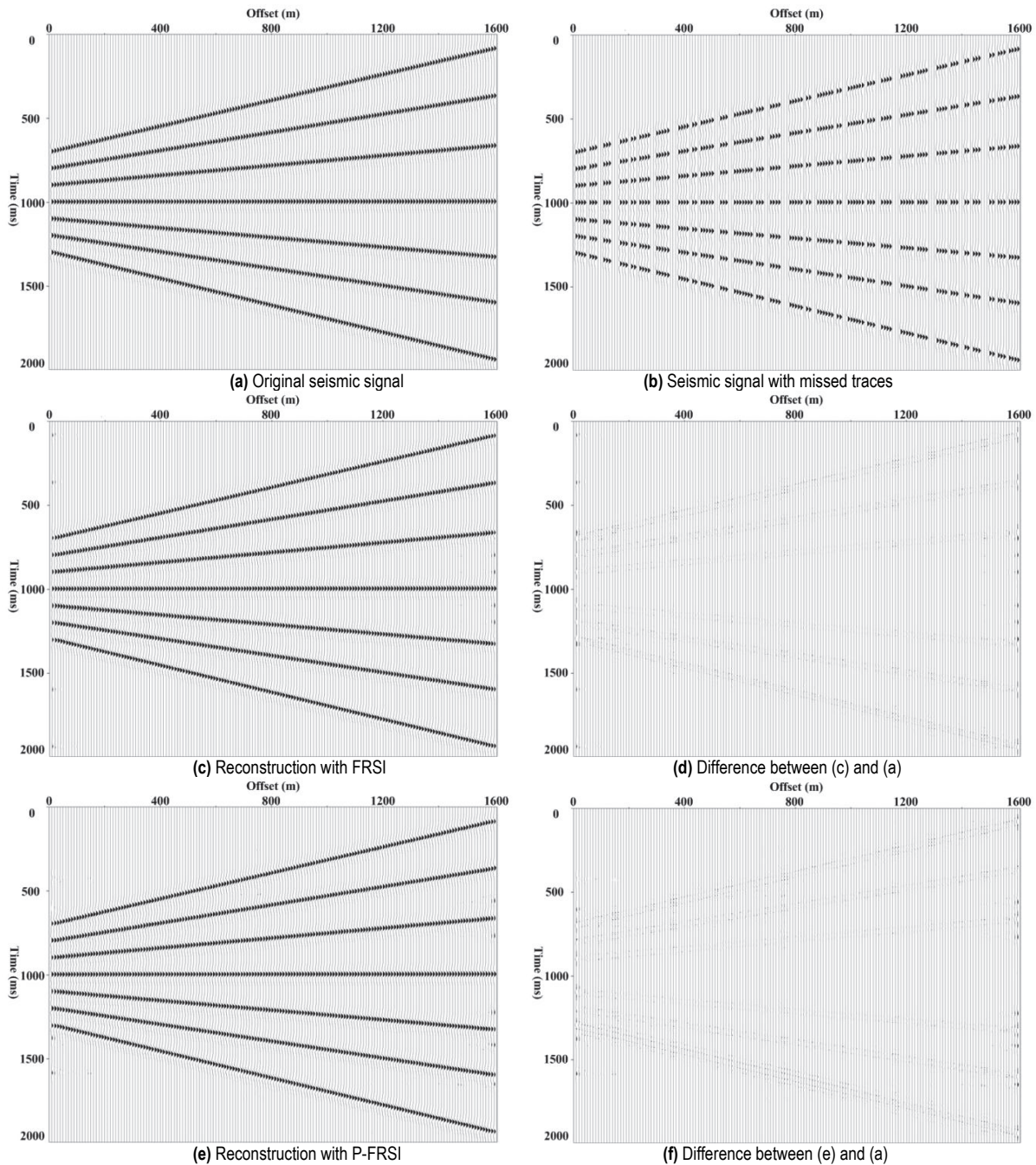


Figure 4 Linear planar seismic signal and its reconstruction results

The signal itself is a theoretical one and the quantity of data is small. We divided the signal into 4 parts, and the overlapped zones are calculated twice or 4 times. And the whole record is split into four blocks ($D_x = 2, D_t = 2$).

The linear superposition is used to splice these 4 blocks to get the final result. Compared to FRSI, P-FRSI needs to adjust every block's parameter. Fig. 4c shows the reconstruction result of FRSI and Fig. 4e shows the result

of P-FRSI. The two results have no distinct difference just through observing Fig. 4c, Fig. 4e. The performances of FRSI and P-FRSI are quite similar, although the details of the P-FRSI result are slightly better.

5.2 Pre-Stack Marine Seismic Signal Reconstruction

In this example, we will do a severe example to confirm the performance of P-FRSI. Fig. 5a shows this 2-

D signal, which was extracted from a marine seismic record. As the experiment needs, the data of the 45 traces in the original 240 traces are deleted randomly, as shown in Fig. 5b. The time interval is set to 1ms and the trace

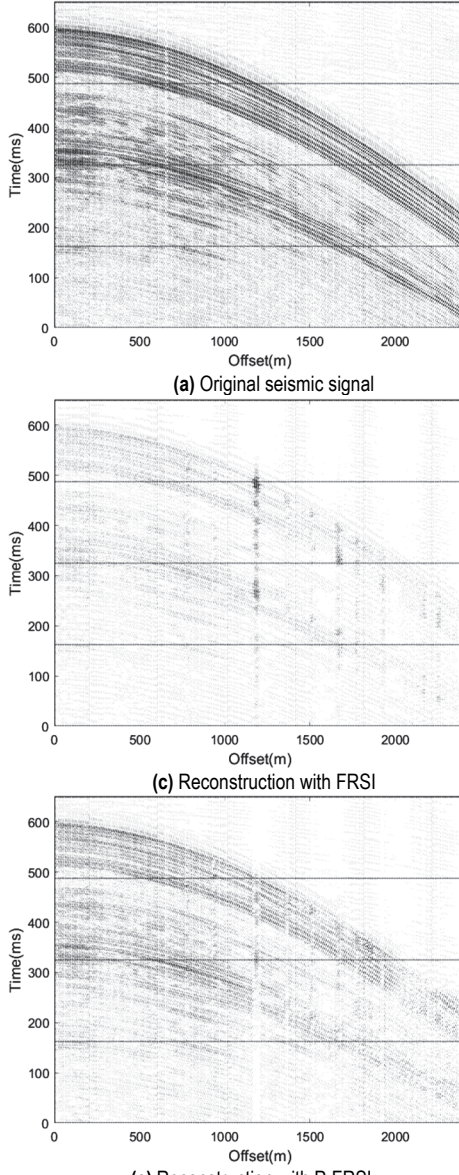
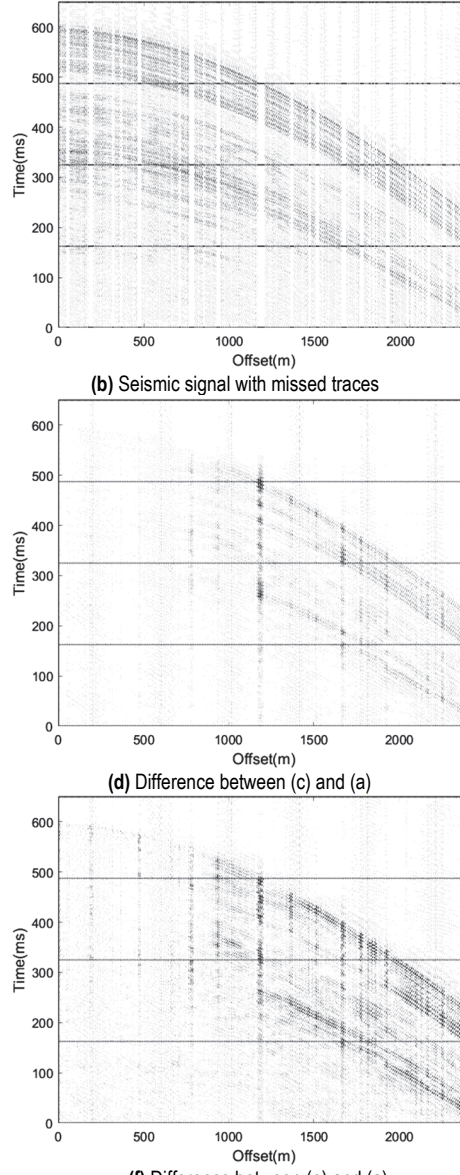


Figure 5 Marine seismic signal and its reconstruction results

In this example, if we want the curved seismic trace to seem to be straight, we would split many parts in the spatial direction. Therefore this signal is divided into 40 blocks ($D_x = 8$, $D_t = 5$) . This means that there is an overlap between blocks and blocks. Fig. 5c gives the FRSI result and Fig. 5e gives the P-FRSI result. Comparing these two Fig. 5c, Fig. 5e by observing 500 m and 1500 m of these two results, because of the limitation of FRSI, the reconstruction result here has spectral aliasing. The P-FRSI reconstruction results, as expected, are much better, and the extreme value of reconstruction error is not so large.

The metrics and runtime of FRSI and P-FRSI are presented below in Tab. 1. In the previous experiments, the linear events had approximately equal energy, but through this severe experiment, we find that P-FRSI has a higher performance than FRSI. P-FRSI is quite able to handle this case despite the quite strong irregularities in the sampling.

spacing is 10m. FRSI was applied by setting parameters of $a = 1$, σ_p^2 was set 10 percentile of the maximal value of NDFT coefficients.



The reconstruction time of P-FRSI is much shorter than FRSI. There are repeated calculations for the partition methods. However, we do not have to reconstruct such big data once. Therefore, P-FRSI runs faster than FRSI when dealing with big data.

Table 1 MSE, Maximum Point Error, and Runtime in Example Two

| Methods | MSE | Maximum Point Error | Runtime / s |
|---------|------|---------------------|-------------|
| FRSI | 0.28 | 11.76 | 24.10 |
| P-FRSI | 0.16 | 5.42 | 15.81 |

5.3 Post-Stack Land Seismic Signal Reconstruction

To further verify the improvement effect of P-FRSI, the following experiment selects a part of the post-stack seismic signal to carry out reconstruction experiments. As can be seen in Fig. 6a, this signal records 2000 m of data in

500 ms. The sampling interval is 1 ms and the trace spacing is 10 m.

In the P-FRSI case, the post-stack land seismic signal is divided into 16 blocks, with $D_x = 4, D_t = 4$. The overlap is 22 and 14 in time and spatial space dimensions respectively. In the figure below, Fig. 6a shows the post-stack land seismic signals, and Fig. 6b shows it with some signals deleted randomly. The difference between the two

reconstruction results in Fig. 6c, Fig. 6e is still too small to distinguish with eyes. So in Fig. 6d, Fig. 6f, we calculated the difference between the results of two different methods and the original signal. The reconstruction result of P-FRSI is found to outperform the FRSI in Fig. 6d, Fig. 6f. Moreover, the RMSE of P-FRSI is significantly smaller than FRSI's and the runtime of P-FRSI is almost half less than FRSI. Therefore, in this case, the performance of P-FRSI is better than FRSI.

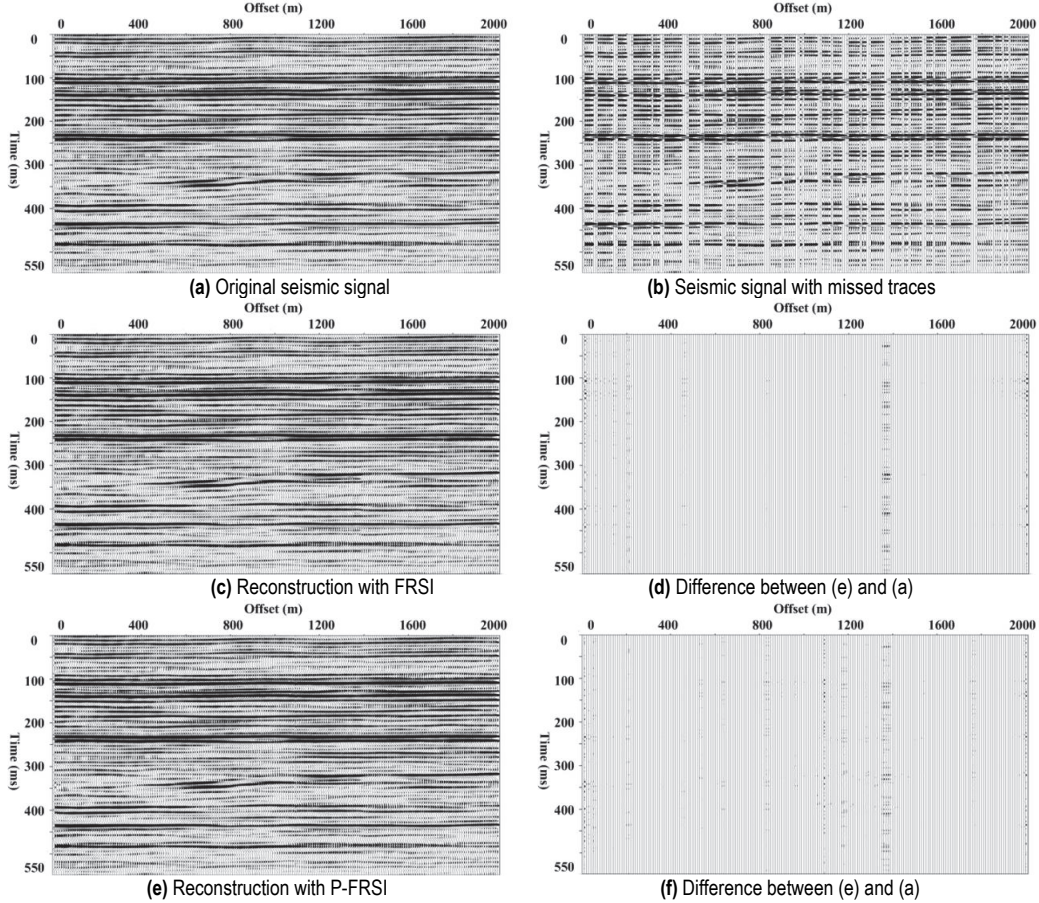


Figure 6 Post-stack land seismic signal and its reconstruction results

6 CONCLUSIONS AND DISCUSSIONS

This paper proposes a new P-FRSI for non-uniform sampling signal reconstruction. The experimental results have shown how FRSI and P-FRSI performed in 2-D seismic signal reconstruction. From the experiments, we get the result as we expected by comparing MSE, maximum point error, and runtime with the result of FRSI. These three aspects also reflect the three features of P-FRSI compared to the standard FRSI. Firstly, the parameter selection is very convenient, in particular, different sub-blocks respond to distinct frequency bandwidth. The second feature is that the proposed method linearizes the curved events to reduce the difficulty of reconstruction. The last feature is that P-FRSI can save reconstruction time. These experiments testify to the good performance of our approach.

The proposed P-FRSI has potential usefulness in seismic signal prediction, and this topic is certainly worthy of further investigation. Future work includes how to improve the reconstruction efficiency of P-FRSI.

Acknowledgements

The research was supported by the Hainan Provincial Natural Science Foundation of China, Grant No: 422MS091, and supported by the Hainan Provincial Joint Project of Sanya Yazhou Bay Science and Technology City, Grant No: 2021CXLH0018, and supported by Hainan Institute Foundation of Zhejiang University.

7 REFERENCES

- [1] Black, H. S. (1953). *Modulation Theory*. New York: Van Nostrand, 120-183.
- [2] Liu, P. & Wang, Y. (2018). Seismic data decomposition and reconstruction with sparse Gaussian beams and sparse optimisation method. *Exploration Geophysics*, 49, 50-57. <https://doi.org/10.1071/EG15114>
- [3] Zhang, H., Wang, D., & Li, H., et al. (2017). High-accurate seismic data reconstruction based on non-uniform curvelet transform. *Chinese Journal of Geophysics*, 60(11), 4480-4490.

- [4] Ronen, S., Sorin, V., & Bale, R. (1991). Spatial dealiasing of 3-D seismic reflection data. *Geophysical Journal International*, 105, 503-511.
<https://doi.org/10.1111/j.1365-246X.1991.tb06729.x>
- [5] Liu, G., Li, C., Guo, Z., & Rao, Y. (2019). Irregularly Sampled Seismic Data Reconstruction Using Multiscale Multidirectional Adaptive Prediction-Error Filter. *IEEE Transactions on Geoscience and Remote Sensing*, 57(5), 2909-2919. <https://doi.org/10.1109/TGRS.2018.2878402>
- [6] Wang, H., Tao, C., & Chen, S., Ziyin, W., Yong, D., Jianping, Z., Lei, Q., Honglei, S., Weijun, X., & Yunlong, L. (2019). High-precision seismic data reconstruction with multi-domain sparsity constraints based on curvelet and high-resolution radon transforms. *Journal of Applied Geophysics*, 162, 128-137.
<https://doi.org/10.1016/j.jappgeo.2018.12.003>
- [7] Carozzi, F. & Sacchi, M. D. (2019). Robust tensor-completion algorithm for 5D seismic-data reconstruction. *Geophysics*, 84, V97-V109.
<https://doi.org/10.1190/geo2018-0109.1>
- [8] Liu, J., Gu, Y., & Chou, Y. (2019). Seismic data reconstruction via complex Shearlet transform and block coordinate relaxation. *Journal of Seismic Exploration*, 28, 307-332.
- [9] Yu, J. & Wu, B. (2022). Attention and Hybrid Loss Guided Deep Learning for Consecutively Missing Seismic Data Reconstruction. *IEEE Transactions on Geoscience and Remote Sensing*, 60, 1-8.
<https://doi.org/10.1109/TGRS.2021.3068279>
- [10] Park, J., Yoon, D., Seol, S. J., & Byun, J. (2019). Reconstruction of seismic field data with convolutional U-Net considering the optimal training input data. *89th Annual International Meeting, SEG, Expanded Abstracts*, 4650-4654. <https://doi.org/10.1190/segam2019-3216017.1>
- [11] Wang, Y., Wang, B., Tu, N., & Geng, J. (2020). Seismic trace interpolation for irregularly spatial sampled data using convolutional auto-encoder. *Geophysics*, 85(2), V119-V130.
<https://doi.org/10.1190/geo2018-0699.1>
- [12] Canning, A. & Gardner, G. H. F. (1996). Regularizing 3D data sets with DMO. *Geophysics*, 61, 1108-1114.
<https://doi.org/10.1190/1.1444031>
- [13] Spitz, S. (1991). Seismic trace interpolation in the F-X domain. *Geophysics*, 56, 785-794.
<https://doi.org/10.1190/1.1443096>
- [14] Hugonnet, P. & Canadas, G. (1997). Regridding of irregular data using 3D Radon decompositions. *67th Annual International Meeting, SEG, Expanded Abstracts*, 1111-1114. <https://doi.org/10.1190/1.1885585>
- [15] Duijndam, A. J. W., Schonewille, M. A., & Hindriks C. O. H. (1999). Reconstruction of band-limited signals, irregularly sampled along one spatial direction. *Geophysics*, 64(2), 524-538. <https://doi.org/10.1190/1.1444559>
- [16] Trad, D., Ulrych, T., & Sacchi, M. D. (2003). Latest views of the sparse Radon transform. *Geophysics*, 68(1), 386-399.
<https://doi.org/10.1190/1.1543224>
- [17] Zwartjes, P. & Gisolf, A. (2006). Fourier reconstruction of marine-streamer data in four spatial coordinates. *Geophysics*, 71(6), 171-186. <https://doi.org/10.1190/1.2348633>
- [18] Font-Segura J., Vázquez G., & Riba J. (2011). Noise enhancement and SNR equivalence in Bernoulli nonuniform sampling. *4th Int. Conf. Cognitive Radio and Advanced Spectrum Management, ACM Int. Conference Proceeding Series*. <https://doi.org/10.1145/2093256.2093270>
- [19] Feizi, S., Angelopoulos, G., & Goyal, V. K. (2011). Energy-efficient time-stampless adaptive non uniform sampling. *10th IEEE Sensors Conference*, 912-915.
<https://doi.org/10.1109/ICSENS.2011.6127202>
- [20] Yan, B., Zhao, J., Zhang, H., et al. (2015). NUFFT-Based Iterative Image Reconstruction via Alternating Direction Total Variation Minimization for Sparse-View CT. *Computational and Mathematical Methods in Medicine*, 2015(3), 1-9. <https://doi.org/10.1109/ICSENS.2011.6127202>
- [21] Liu, L., Plonka, G., & Ma, J. (2017). Seismic data interpolation and denoising by learning a tensor tight frame. *Inverse Problems*, 33(10).
<https://doi.org/10.1088/1361-6420/aa7773>
- [22] Liu, B. & Sacchi, M. D. (2001). Minimum weighted norm interpolation of seismic data with adaptive weight. *71st Annual International Meeting, SEG, Expanded Abstracts*, 1921-1924. <https://doi.org/10.1190/1.1836829>
- [23] Sacchi, M. D. & Ulrych, T. J. (1996). Estimation of the discrete Fourier transform, a linear inversion approach. *Geophysics*, 61(4), 1128-1136.
<https://doi.org/10.1190/1.1444033>
- [24] Wang, Y. (2003). Sparseness-constrained least-squares inversions: Application to seismic wave reconstruction. *Geophysicists*, 68(5), 1633-1638.
<https://doi.org/10.1190/1.1620637>
- [25] Hindriks, K. & Duijndam, A. J. W. (2000). Reconstruction of 3D seismic signals irregularly sampled along twospatial coordinates. *Geophysics*, 65, 253-263.
<https://doi.org/10.1190/1.1444716>
- [26] Zwartjes, P. & Gisolf, A. (2007). Fourier reconstruction with sparse inversion. *Geophysical Prospecting*, 55, 199-221.
<https://doi.org/10.1111/j.1365-2478.2006.00580.x>
- [27] Zwartjes P. M. & Sacchi M. D. (2007). Fourier reconstruction of non-uniformly sampled, aliased seismic data. *Geophysics*, 72(1), 21-32.
<https://doi.org/10.1190/1.2399442>
- [28] Oppenheim, A. V., Schafer, R. W., & Buck, J. R. (1999). *Discrete-time signal processing* (2nd ed.). Prentice-Hall, Inc.
- [29] Nyquist, H. (1928). Certain topics in telegraph transmission theory. *Proceedings of the IEEE*, 90(2), 280-305.
<https://doi.org/10.1109/5.989875>
- [30] Duijndam, A. J. W. & Schonewille, M. A. (1999). Nonuniform fast Fourier transform. *Geophysics*, 64, 539-551. <https://doi.org/10.1190/1.1444560>
- [31] Liu, S., Yan, Z., & Zhu, W., Bingkai, H., Hanming, G., & Shanzheng, H. (2021). An illumination-compensated Gaussian beam migration for enhancing subsalt imaging. *Geophysical Prospecting*, 69, 1433-1440.
<https://doi.org/10.1111/1365-2478.13117>
- [32] Feichtinger, H., Gröchenig, K., & Strohmer, T. (1995). Efficient numerical methods in nonuniform sampling theory. *Numerische Mathematik*, 69, 423-440.
<https://doi.org/10.1007/s002110050101>
- [33] Candès, E. J. (2006). Compressive Sampling. *Marta Sanz Solé*, 17(2), 1433-1452. <https://doi.org/10.4171/022-3/69>

Contact information:

Zhaolin ZHU, Professor of Engineering, PhD
Hainan Institute of Zhejiang University,
11# Building, Yongyou Industrial Park,
Yazhou Bay Science and Technology City,
Yazhou District, Sanya City, Hainan Province 572025, P.R. China
E-mail: zhuzhaolin@zju.edu.cn

Haoran REN, Associate Professor, PhD
(Corresponding author)
Zhejiang University,
154# Yugu Road,
Xihu District, Hangzhou City,
Zhejiang Province 310027, P.R. China
E-mail: rhr@zju.edu.cn

Liurong TAO, Postgraduate Student
Zhejiang University,
154# Yugu Road,
Xihu District, Hangzhou City,
Zhejiang Province 310027, P.R. China
E-mail: taolr@zju.edu.cn

Jinsheng JIANG, PhD Student
Zhejiang University,
154# Yugu Road,
Xihu District, Hangzhou City,
Zhejiang Province 310027, P.R. China
E-mail: jiangjs217@zju.edu.cn

Tong WANG, Postgraduate Student
Zhejiang University,
154# Yugu Road,
Xihu District, Hangzhou City,
Zhejiang Province 310027, P.R. China
E-mail: 22138015@zju.edu.cn

Mingxin CHENG, PhD Student
Zhejiang University,
154# Yugu Road,
Xihu District, Hangzhou City,
Zhejiang Province 310027, P.R. China
E-mail: mingxincheng@zju.edu.cn

Shuaimin DING, Postgraduate Student
Zhejiang University,
154# Yugu Road,
Xihu District, Hangzhou City,
Zhejiang Province 310027, P.R. China
E-mail: smding@zju.edu.cn

Rui DU, Postgraduate Student
Zhejiang University,
154# Yugu Road,
Xihu District, Hangzhou City,
Zhejiang Province 310027, P.R. China
E-mail: 22034060@zju.edu.cn